

Microwave Linear Analog Computer (MiLAC) for Simultaneous Active and Passive Beamforming

Matteo Nerini, *Member, IEEE*, Bruno Clerckx, *Fellow, IEEE*

Abstract—Microwave linear analog computers (MiLACs) have recently emerged to enable high-performance and efficient beamforming in the analog domain. In this paper, we introduce a dual-functionality framework for MiLAC-aided transceivers. Beyond analog-domain precoding/combining (active beamforming), a MiLAC and its antenna array can simultaneously act as a reconfigurable intelligent surface (RIS) (passive beamforming). This allows the MiLAC to execute beamforming for transmission/reception while reflecting external incident signals. We provide an optimal reconfiguration strategy for this dual-functional MiLAC, and characterize the fundamental limits on the trade-off between active and passive rate, namely the capacity region bounds and the sum-rate capacity.

Index Terms—Beamforming, microwave linear analog computer (MiLAC), reconfigurable intelligent surface (RIS).

I. INTRODUCTION

Microwave linear analog computer (MiLAC) has been proposed to enable high-performance beamforming purely in the analog domain by processing the signals via a reconfigurable microwave network [1]. In a MiLAC-aided transmitter, the MiLAC receives as input the transmitted symbols from the radio frequency (RF) chains, precodes them in the analog domain, and returns the precoded signals to the antennas. In a MiLAC-aided receiver, the MiLAC receives the inputs from the receiving antennas, combines them in the analog domain, and sends the processed signals to the RF chains for baseband detection. This analog architecture offers a scalable solution towards large-scale multiple-input multiple-output (MIMO) for single-user communications [2], multi-user communications [3], [4], [5], [6], and radar sensing [7].

Reconfigurable microwave networks have also been widely investigated to implement reconfigurable intelligent surfaces (RISs) [8], [9]. By dynamically adjusting their electromagnetic (EM) properties, RISs can control the reflection of incident signals through passive beamforming. RISs have been implemented conventionally with reconfigurable loads connected to antenna elements. Nevertheless, they can also be implemented with more general microwave networks, such as those in MiLAC, and the resulting RIS architectures are denoted as simultaneously transmitting and reflecting RIS (STAR-RIS) [10] and beyond-diagonal RIS (BD-RIS) [11].

In this work, we bridge MiLAC and RIS by arguing that a MiLAC mounted on a transceiver device can perform a second function in addition to precoding/combining. When the antenna array connected to the MiLAC is sufficiently large, it

can also serve as a BD-RIS, reflecting incident signals coming from external transmitting devices toward their intended receivers. Consequently, we introduce a dual-functionality framework where a MiLAC can simultaneously execute active beamforming (precoding/combining signals from/to its RF chains) and passive beamforming (reflecting external incident signals to desired directions).

To illustrate the utility of this dual functionality, four exemplary wireless scenarios are shown in Fig. 1. In Fig. 1(a), the MiLAC transmits a signal to User 1, which operates in full-duplex and in turn transmits to User 2. Therefore, the MiLAC simultaneously performs active beamforming toward User 1 and passive beamforming to help the communication from User 1 to 2. In Fig. 1(b), the MiLAC receives the signal from User 1, which operates in full-duplex and in turn receives from User 2. Here, the MiLAC simultaneously performs active beamforming toward User 1 and passive beamforming to aid the communication from User 2 to 1. In Fig. 1(c), the MiLAC transmits a signal to User 1, which also receives the signal from User 2. Hence, the MiLAC simultaneously performs active beamforming toward User 1 and passive beamforming to support the communication from User 2 to 1. In Fig. 1(d), the MiLAC receives the signal from User 1, which also transmits to User 2. Here, the MiLAC simultaneously performs active beamforming toward User 1 and passive beamforming to aid the communication from User 1 to 2.¹

When a MiLAC is implemented with lossless and reciprocal hardware, its scattering matrix is unitary and symmetric. This couples the transmissive and reflective capabilities of the MiLAC, creating a trade-off between the rates achievable by active and passive beamforming. In this work, we explore the fundamental limits of this trade-off, and make the following contributions. *First*, we establish a system model for dual-functional MiLAC-aided transceivers and provide the expressions of the active and passive achievable rates. *Second*, we derive tight upper bounds on both rates, and show that they cannot be achieved simultaneously. Therefore, we characterize in closed form their capacity region, i.e., the set of all rate pairs that are simultaneously achievable, and the sum-rate capacity. *Third*, we provide a global-optimal solution to optimize the MiLAC to operate on the frontier of the capacity region and achieve the sum-rate capacity, and report simulation results that confirm the theoretical insights.

¹Although the full-duplex scenarios in Fig. 1 resemble the scenario studied in [12] to highlight the benefits of non-reciprocal BD-RIS, there is a fundamental difference. Here, one stream is transmitted through the MiLAC and the other is reflected, while in [12] both streams are reflected by the BD-RIS. As a result, a reciprocal MiLAC can achieve maximum performance here: none of the performance bounds derived in this paper can be improved by relaxing the symmetry constraints on the MiLAC scattering matrix.

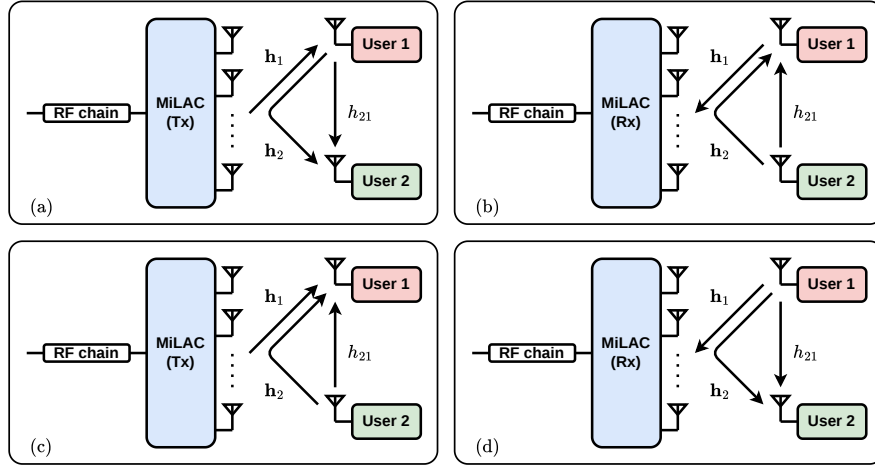


Fig. 1. Four wireless systems where MiLAC performs simultaneous active and passive beamforming.

II. SYSTEM MODEL

To showcase the capability of MiLAC to support active and passive beamforming simultaneously, we consider the communication system represented in Fig. 1(a) throughout the work. In Fig. 1(a), an N -antenna transmitter equipped with a MiLAC communicates with a single-antenna user, denoted as User 1. At the same time, User 1 operates in full-duplex mode and transmits to a second single-antenna user, denoted as User 2. The objective is to reconfigure the MiLAC such that it simultaneously performs beamforming toward User 1 (active beamforming), and reflects the signal transmitted by User 1 toward User 2 (passive beamforming).

Since the MiLAC-aided transmitter sends a single stream of information, it only has a single RF chain [2]. Therefore, the MiLAC microwave network has one input port and N output ports, for a total of $N + 1$ ports, and can be characterized by its scattering matrix $\bar{\Theta} \in \mathbb{C}^{(N+1) \times (N+1)}$ [13]. Under the common assumption that the MiLAC microwave network is implemented with lossless and reciprocal components, its scattering matrix is constrained to be unitary and symmetric, i.e., $\bar{\Theta}^H \bar{\Theta} = \mathbf{I}$ and $\bar{\Theta} = \bar{\Theta}^T$. Furthermore, it can be conveniently partitioned as

$$\bar{\Theta} = \begin{bmatrix} \theta & \boldsymbol{\theta}^T \\ \boldsymbol{\theta} & \Theta \end{bmatrix}, \quad (1)$$

where $\theta \in \mathbb{C}$ is the reflection coefficient at port 1, $\boldsymbol{\theta} \in \mathbb{C}^{N \times 1}$ is the transmission scattering matrix from port 1 to the N ports connected to the N antennas, and $\Theta \in \mathbb{C}^{N \times N}$. We now illustrate how $\bar{\Theta}$ affects the communication between MiLAC and User 1, and between User 1 and 2. In this work, all signals are RF narrowband signals and are represented through their complex baseband equivalent.

Denote as $s_M \in \mathbb{C}$ the symbol sent by the MiLAC-aided transmitter, i.e., at the output of its RF chain, and as $y_1 \in \mathbb{C}$ the corresponding received signal at User 1. Following [2], the signal y_1 is given by

$$y_1 = \mathbf{h}_1^T \boldsymbol{\theta} x_M + n_1, \quad (2)$$

where $\mathbf{h}_1 \in \mathbb{C}^{N \times 1}$ is the channel from User 1 and the MiLAC, $x_M = s_M/2$, and $n_1 \sim \mathcal{CN}(0, \sigma_1^2)$ is the additive white Gaussian noise (AWGN) at User 1 with power σ_1^2 . To understand how the MiLAC scattering matrix $\bar{\Theta}$ impacts y_1 , we equivalently rewrite (2) as

$$y_1 = \bar{\mathbf{h}}_1^T \bar{\Theta} \mathbf{b} x_M + n_1, \quad (3)$$

where $\bar{\mathbf{h}}_1 = [0, \mathbf{h}_1^T]^T \in \mathbb{C}^{(N+1) \times 1}$ and $\mathbf{b} = [1, 0, \dots, 0]^T \in \mathbb{C}^{(N+1) \times 1}$, where we explicitly highlight $\bar{\Theta}$. Following (2) and (3), the rate achieved between the MiLAC and User 1 is

$$R_1 = \log_2 \left(1 + P_M \frac{|\mathbf{h}_1^T \boldsymbol{\theta}|^2}{\sigma_1^2} \right) \quad (4)$$

$$= \log_2 \left(1 + P_M \frac{|\bar{\mathbf{h}}_1^T \bar{\Theta} \mathbf{b}|^2}{\sigma_1^2} \right), \quad (5)$$

where $P_M = \mathbb{E}[|x_M|^2] = \mathbb{E}[|s_M|^2]/4$ is the transmit power.

Similarly, denote as $x_1 \in \mathbb{C}$ the signal transmitted by User 1 and as $y_2 \in \mathbb{C}$ the corresponding received signal at User 2. The signal y_2 writes as

$$y_2 = (h_{21} + \mathbf{h}_2^T \Theta \mathbf{h}_1) x_1 + n_2, \quad (6)$$

where $h_{21} \in \mathbb{C}$ is the direct channel from User 1 to 2, $\mathbf{h}_2 \in \mathbb{C}^{N \times 1}$ is the channel from User 2 to the MiLAC, and $n_2 \sim \mathcal{CN}(0, \sigma_2^2)$ is the AWGN at User 2 with power σ_2^2 . To highlight the role of the MiLAC scattering matrix $\bar{\Theta}$, (6) can also be written as

$$y_2 = (h_{21} + \bar{\mathbf{h}}_2^T \bar{\Theta} \bar{\mathbf{h}}_1) x_1 + n_2, \quad (7)$$

where $\bar{\mathbf{h}}_2 = [0, \mathbf{h}_2^T]^T \in \mathbb{C}^{(N+1) \times 1}$. From (6) and (7), the rate achieved between User 1 and 2 is

$$R_2 = \log_2 \left(1 + P_1 \frac{|h_{21} + \mathbf{h}_2^T \Theta \mathbf{h}_1|^2}{\sigma_2^2} \right) \quad (8)$$

$$= \log_2 \left(1 + P_1 \frac{|h_{21} + \bar{\mathbf{h}}_2^T \bar{\Theta} \bar{\mathbf{h}}_1|^2}{\sigma_2^2} \right), \quad (9)$$

where $P_1 = \mathbb{E}[|x_1|^2]$ is the transmit power.

III. MiLAC OPTIMIZATION

When reconfiguring the MiLAC, our objective is to optimize $\bar{\Theta}$ subject to the unitary and symmetric constraints to simultaneously maximize the two rates R_1 and R_2 . In this section, we first optimize $\bar{\Theta}$ to individually maximize R_1 and R_2 . Second, we characterize the capacity region, i.e., the set of all rate pairs (R_1, R_2) that are simultaneously achievable. Third, we maximize the sum-rate $R = R_1 + R_2$.

A. Individual Rate Maximization

Two opposite working modes can be identified for the MiLAC. In the first mode, it is used purely for active beamforming, i.e., to precode the symbol x_M for User 1. In this case, we want to maximize R_1 , which is upper bounded by

$$\bar{R}_1 = \log_2 \left(1 + P_M \frac{\|\mathbf{h}_1\|^2}{\sigma_1^2} \right), \quad (10)$$

according to the Cauchy-Schwarz inequality applied to (4) and because $\|\boldsymbol{\theta}\| \leq 1$. This upper bound can be exactly achieved if and only if $\boldsymbol{\theta}$ is designed such that

$$\frac{\mathbf{h}_1^T}{\|\mathbf{h}_1\|} \boldsymbol{\theta} = 1, \quad (11)$$

as it can be noticed from (4), or, equivalently, if and only if

$$\bar{\Theta} \frac{\bar{\mathbf{h}}_1}{\|\mathbf{h}_1\|} = \mathbf{b}, \quad (12)$$

as it can be seen from (5). Condition (12) can be satisfied by optimizing the unitary and symmetric matrix $\bar{\Theta}$ with [14, Alg. 1], which was developed for BD-RIS, as a function of $\bar{\mathbf{h}}_1/\|\mathbf{h}_1\|$ and \mathbf{b} .

In the second mode, the MiLAC is used purely for passive beamforming, i.e., to enhance the link between User 1 and 2. Here, we want to maximize R_2 , which is upper bounded by

$$\bar{R}_2 = \log_2 \left(1 + P_1 \frac{(|h_{21}| + \|\mathbf{h}_2\| \|\mathbf{h}_1\|)^2}{\sigma_2^2} \right), \quad (13)$$

following the Cauchy-Schwarz and triangle inequalities applied to (8) and because $\|\bar{\Theta}\| \leq 1$. This upper bound can be exactly achieved if and only if $\bar{\Theta}$ is designed such that

$$\bar{\Theta} \frac{\mathbf{h}_1}{\|\mathbf{h}_1\|} = \frac{\bar{\mathbf{h}}_2^*}{\|\mathbf{h}_2\|} e^{j \arg(h_{21})}, \quad (14)$$

as it can be noticed from (8), or, equivalently, if and only if

$$\bar{\Theta} \frac{\bar{\mathbf{h}}_1}{\|\mathbf{h}_1\|} = \frac{\bar{\mathbf{h}}_2^*}{\|\mathbf{h}_2\|} e^{j \arg(h_{21})}, \quad (15)$$

as it can be seen from (9). As for (12), condition (15) can be achieved by optimizing $\bar{\Theta}$ with [14, Alg. 1].

We have derived sufficient and necessary conditions on $\bar{\Theta}$ to maximize the two rates R_1 and R_2 in (12) and (15), respectively. These two conditions have the same left-hand side but orthogonal right-hand side (recall that \mathbf{b} is zero everywhere except in its first entry, while $\bar{\mathbf{h}}_2$ has a zero first entry). Thus, the two rates R_1 and R_2 cannot be simultaneously maximized. If R_1 is maximized, i.e., $R_1 = \bar{R}_1$, then $R_2 = \underline{R}_2$, with $\underline{R}_2 = \log_2(1 + P_1 |h_{21}|^2 / \sigma_2^2)$, which is obtained by substituting

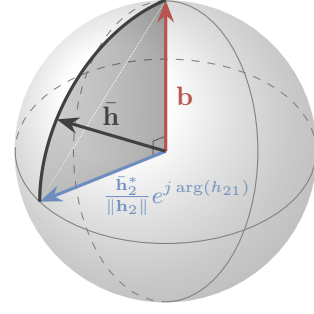


Fig. 2. The unit N -sphere, the orthonormal vectors $\bar{\mathbf{h}}_2^*/\|\mathbf{h}_2\| e^{j \arg(h_{21})}$ and $\mathbf{b} = [1, 0, \dots, 0]^T$, and the shortest arc connecting them.

(12) into (9) and is the rate R_2 achievable by only using the direct link h_{21} between User 1 and 2. If R_2 is maximized, i.e., $R_2 = \bar{R}_2$, then $R_1 = 0$, as obtained by plugging (15) into (5).

B. Capacity Region Characterization

Since R_1 and R_2 cannot be simultaneously maximized, the sum-rate upper bound $\bar{R} = \bar{R}_1 + \bar{R}_2$ cannot be reached. Thus, there exists a trade-off between the rates R_1 and R_2 that can be achieved. Formally, this trade-off is given by the capacity region \mathcal{C} , i.e., the set of all rate pairs (R_1, R_2) that are simultaneously achievable. In the following, we characterize the frontier of such a region.

We begin by giving an intuition on how the MiLAC should be reconfigured to operate on the frontier of the capacity region, and then provide a formal proof to show that this intuitive design is optimal. The rates R_1 and R_2 are individually maximized if conditions (12) and (15) are fulfilled, respectively. Since it is impossible to fulfill both of them simultaneously, we can impose a compromise

$$\bar{\Theta} \frac{\bar{\mathbf{h}}_1}{\|\mathbf{h}_1\|} = \bar{\mathbf{h}}, \quad (16)$$

where $\bar{\mathbf{h}} \in \mathbb{C}^{(N+1) \times 1}$ is introduced as

$$\bar{\mathbf{h}} = t \frac{\bar{\mathbf{h}}_2^*}{\|\mathbf{h}_2\|} e^{j \arg(h_{21})} + \sqrt{1-t^2} \mathbf{b}, \quad (17)$$

depending on a parameter $t \in [0, 1]$. Note that $\bar{\mathbf{h}}$ is a unit-norm vector that always lies on the shortest arc of the unit N -sphere connecting $\bar{\mathbf{h}}_2^*/\|\mathbf{h}_2\| e^{j \arg(h_{21})}$ and \mathbf{b} , as illustrated in Fig. 2. Since $\bar{\mathbf{h}}$ has unit norm, condition (16) can always be fulfilled by optimizing $\bar{\Theta}$ with [14, Alg. 1]. For $t = 0$, condition (16) boils down to (12) and R_1 is maximized; for $t = 1$, condition (16) boils down to (15) and R_2 is maximized; and for other values of t , we achieve

$$R_1(t) = \log_2 \left(1 + P_M \frac{\|\mathbf{h}_1\|^2 (1-t^2)}{\sigma_1^2} \right), \quad (18)$$

$$R_2(t) = \log_2 \left(1 + P_1 \frac{(|h_{21}| + \|\mathbf{h}_2\| \|\mathbf{h}_1\| t)^2}{\sigma_2^2} \right), \quad (19)$$

which can be shown by substituting (16) into (5) and (9). Interestingly, these two parametric expressions of $R_1(t)$ and $R_2(t)$ identify the frontier of the capacity region, as formalized in the following proposition.

Proposition 1. *The frontier of the capacity region containing all possible pairs (R_1, R_2) is given by the curve identified by the parametric expressions (18) and (19), for $t \in [0, 1]$.*

Proof. We prove the proposition by showing that: *i)* if $R_2(t)$ is achieved for some $t \in [0, 1]$, then $R_1 \leq R_1(t)$, and *ii)* if $R_1(t)$ is achieved for some $t \in [0, 1]$, then $R_2 \leq R_2(t)$.

First, achieving $R_2(t)$ implies that

$$\left| \hat{\mathbf{h}}_1^T \hat{\mathbf{h}}_2 \right| = t, \quad (20)$$

where we introduced $\hat{\mathbf{h}}_1 = \bar{\mathbf{O}}\bar{\mathbf{h}}_1/\|\mathbf{h}_1\|$ and $\hat{\mathbf{h}}_2 = \bar{\mathbf{h}}_2/\|\mathbf{h}_2\|$. We now use the Parseval's identity to express $\|\hat{\mathbf{h}}_1\|^2$ as

$$\left\| \hat{\mathbf{h}}_1 \right\|^2 = \sum_{\mathbf{v} \in \mathcal{B}} \left| \hat{\mathbf{h}}_1^T \mathbf{v} \right|^2, \quad (21)$$

where $\mathcal{B} = \{\mathbf{v}_1, \dots, \mathbf{v}_{N+1}\}$ is any orthonormal basis of \mathbb{C}^{N+1} , with $\mathbf{v}_n \in \mathbb{C}^{N+1 \times 1}$ for $n = 1, \dots, N+1$. We construct such a basis \mathcal{B} as

$$\mathcal{B} = \left\{ \hat{\mathbf{h}}_2, \mathbf{b}, \mathbf{v}_3, \dots, \mathbf{v}_{N+1} \right\}, \quad (22)$$

where $\mathbf{v}_3, \dots, \mathbf{v}_{N+1}$ are orthonormal vectors orthogonal to $\hat{\mathbf{h}}_2$ and \mathbf{b} . Note that (22) is a valid basis since $\hat{\mathbf{h}}_2$ and \mathbf{b} are orthonormal. Recalling that $\|\hat{\mathbf{h}}_1\|^2 = 1$ and applying the Parseval's identity to rewrite $\|\hat{\mathbf{h}}_1\|^2$ as in (21), we obtain

$$1 = \left| \hat{\mathbf{h}}_1^T \hat{\mathbf{h}}_2 \right|^2 + \left| \hat{\mathbf{h}}_1^T \mathbf{b} \right|^2 + \sum_{n=3}^{N+1} \left| \hat{\mathbf{h}}_1^T \mathbf{v}_n \right|^2 \quad (23)$$

$$\geq \left| \hat{\mathbf{h}}_1^T \hat{\mathbf{h}}_2 \right|^2 + \left| \hat{\mathbf{h}}_1^T \mathbf{b} \right|^2. \quad (24)$$

Substituting (20) into (24), we obtain $\left| \hat{\mathbf{h}}_1^T \mathbf{b} \right| \leq \sqrt{1-t^2}$, giving $R_1 \leq R_1(t)$. Second, achieving $R_1(t)$ implies that

$$\left| \hat{\mathbf{h}}_1^T \mathbf{b} \right| = \sqrt{1-t^2}. \quad (25)$$

Similarly to the previous discussion, substituting (25) into (24), we obtain $\left| \hat{\mathbf{h}}_1^T \hat{\mathbf{h}}_2 \right| \leq t$, giving $R_2 \leq R_2(t)$. \square

We can reach all points on the capacity region frontier depending on the parameter $t \in [0, 1]$. If $t = 0$, the MiLAC is used purely for active beamforming (as a transmitter); if $t = 1$, it is used purely for passive beamforming (as a BD-RIS); and if $t \in (0, 1)$, it is used for active and passive beamforming simultaneously (which is reminiscent of a STAR-RIS).

C. Sum-Rate Maximization

Among all the points on the capacity region, we are interested in the sum-rate capacity C defined as the maximum achievable sum of rates $C = \max_{(R_1, R_2) \in \mathcal{C}} R_1 + R_2$. Since the sum-rate capacity lies on the capacity region frontier given by (18) and (19), we want to find the optimal value of $t \in [0, 1]$, called t^* , that maximizes the sum-rate $R(t) = R_1(t) + R_2(t)$. To this end, we find all stationary points of $R(t)$ for $t \in [0, 1]$. It can be shown that solving $dR(t)/dt = 0$ is equivalent to finding the roots of the cubic equation

$$at^3 + bt^2 + ct + d = 0, \quad (26)$$

where

$$a = 2P_1 P_M \|\mathbf{h}_1\|^3 \|\mathbf{h}_2\|^2 \quad (27)$$

$$b = 3P_1 P_M \|\mathbf{h}_1\|^2 \|\mathbf{h}_2\| |h_{21}| \quad (28)$$

$$c = P_M \|\mathbf{h}_1\| \left(P_1 |h_{21}|^2 + \sigma_2^2 \right) \quad (29)$$

$$-P_1 \|\mathbf{h}_1\| \|\mathbf{h}_2\|^2 \left(P_M \|\mathbf{h}_1\|^2 + \sigma_1^2 \right) \quad (30)$$

$$d = -P_1 \|\mathbf{h}_2\| |h_{21}| \left(P_M \|\mathbf{h}_1\|^2 + \sigma_1^2 \right). \quad (31)$$

Thus, there are always up to five candidate values for t^* , given by the real roots of (26) lying in the interval $[0, 1]$, which are up to three, together with the extreme values 0 and 1. After solving (26), the optimal t^* can be readily found by evaluating $R(t)$ in these candidate points.

In the case the direct link between User 1 and 2 is highly obstructed, i.e., $h_{21} = 0$, (26) boils down to $t(at^2 + c) = 0$ since $b = 0$ and $d = 0$. This equation has at most two real solutions in the interval $[0, 1]$, namely $t = 0$ and

$$t = \sqrt{\frac{-c}{a}} = \sqrt{\frac{P_1 \|\mathbf{h}_2\|^2 \left(P_M \|\mathbf{h}_1\|^2 + \sigma_1^2 \right) - P_M \sigma_2^2}{2P_1 P_M \|\mathbf{h}_1\|^2 \|\mathbf{h}_2\|^2}}, \quad (32)$$

the second of which could not be real. If $h_{21} = 0$ and we are in the high-signal-to-noise ratio (SNR) regime, i.e., $P_M \|\mathbf{h}_1\|^2 \gg \sigma_1^2$ and $P_1 \|\mathbf{h}_1\|^2 \|\mathbf{h}_2\|^2 \gg \sigma_2^2$, then (32) simplifies to $t \approx \sqrt{1/2}$. Therefore, in this case, there are three candidate values for t^* , namely $t \in \{0, \sqrt{1/2}, 1\}$. Comparing $R(0)$, $R(\sqrt{1/2})$, and $R(1)$ when $h_{21} = 0$ and we are at high-SNR regime, it is simple to show that the optimal t is $t^* = \sqrt{1/2}$. This is aligned with the fact that at high-SNR uniform power allocation is optimal and offers a multiplexing gain of 2, rather than 1 (which is offered by the extreme $t = 0$ and $t = 1$).

IV. NUMERICAL RESULTS

In this section, we provide numerical results to validate our theoretical insights. We consider independent and identically distributed (i.i.d.) Rayleigh distributed channels, i.e., $h_{21} \sim \mathcal{CN}(0, g_{21})$, $\mathbf{h}_1 \sim \mathcal{CN}(\mathbf{0}, g_1 \mathbf{I})$, and $\mathbf{h}_2 \sim \mathcal{CN}(\mathbf{0}, g_2 \mathbf{I})$, with path gains $g_{21} = 10^{-12}$, and $g_1 = 10^{-7}$, and $g_2 = 10^{-7}$. We set the number of antennas at the MiLAC to $N = 64$, the transmit powers to $P_1 = 10$ dB and $P_M = 10$ dBm, and the noise powers to $\sigma_1^2 = \sigma_2^2 = -80$ dBm.

Fig. 3 shows the capacity region of the achievable pairs (R_1, R_2) . The corner points (\bar{R}_1, \bar{R}_2) and $(0, \bar{R}_2)$ are achieved by using the MiLAC purely for active or passive beamforming, respectively, as described in Section III-A. By time-sharing between these two operating modes, all points on the dashed line can be achieved, obtaining a multiplexing gain of 1 only. Significantly better performance can be achieved by reconfiguring the MiLAC according to the approach in Section III-B. By reconfiguring the MiLAC to satisfy condition (16) for $t \in [0, 1]$, all points on the capacity region frontier can be achieved, as described by the parametric expressions (18) and (19). The sum-rate capacity is achieved with $t = t^*$, on the point $(R_1(t^*), R_2(t^*))$, as described in Section III-C. Since, $t^* \approx \sqrt{1/2}$ (as theoretically proved for when $h_{21} = 0$ and

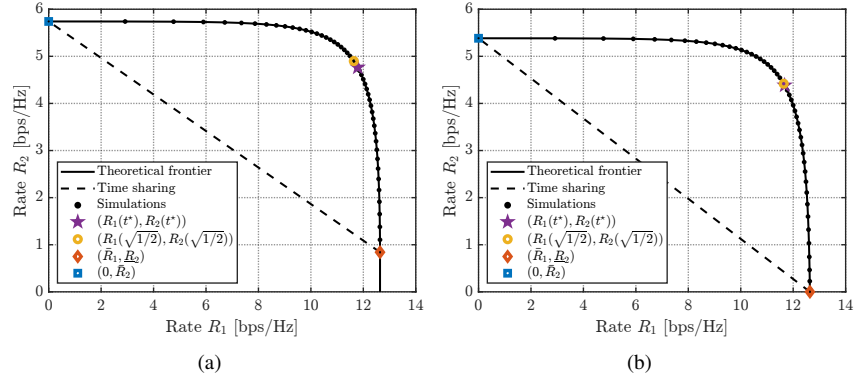


Fig. 3. Capacity region (a) with and (b) without direct link h_{21} .

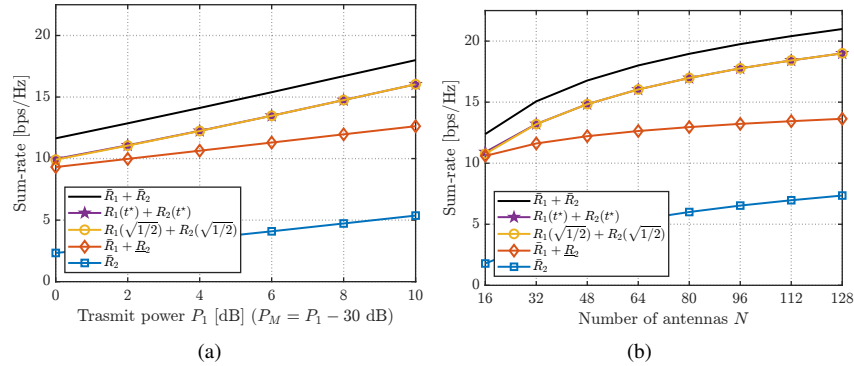


Fig. 4. Sum-rate versus (a) the transmit power P_1 and (b) the number of antennas N at the MiLAC, without direct link h_{21} .

we are in the high-SNR regime), the point $(R_1(t^*), R_2(t^*))$ approximately corresponds to $(R_1(\sqrt{1/2}), R_2(\sqrt{1/2}))$.

Fig. 4 shows the sum-rate $R = R_1 + R_2$ obtained by operating at specific values of the parameter t , compared to the sum-rate upper bound $\bar{R} = \bar{R}_1 + \bar{R}_2$. The curves $\bar{R}_1 + \bar{R}_2$ and \bar{R}_2 are the sum-rates achievable by using the MiLAC purely for active or passive beamforming, respectively, i.e., with $t = 0$ or $t = 1$. By simultaneously using the MiLAC for active and passive beamforming, the sum-rate capacity can be achieved with $t = t^*$, which approximately corresponds to the sum-rate with $t = \sqrt{1/2}$. Although the upper bound \bar{R} cannot be achieved, it is nearly reached by the sum-rate capacity, which has a multiplexing gain of 2 unlike $\bar{R}_1 + \bar{R}_2$ and \bar{R}_2 .

V. CONCLUSION

We propose a dual-functionality framework for transceivers equipped with a MiLAC. In this framework, a MiLAC can simultaneously execute active beamforming for transmission/reception and passive beamforming for reflecting external signals, as a BD-RIS. Due to the unitary and symmetric constraints of lossless and reciprocal MiLACs, a fundamental trade-off exists between these two operating modes. We characterize the limits of this trade-off by deriving the system's capacity region and providing an optimal reconfiguration strategy to achieve sum-rate capacity.

REFERENCES

- [1] M. Nerini and B. Clerckx, "Analog computing for signal processing and communications – Part II: Toward gigantic MIMO beamforming," *IEEE Trans. Signal Process.*, vol. 73, pp. 5198–5212, 2025.
- [2] M. Nerini and B. Clerckx, "Capacity of MIMO systems aided by microwave linear analog computers (MiLACs)," *arXiv preprint arXiv:2506.05983*, 2025.
- [3] T. Fang, X. Zhou, and Y. Mao, "On the performance of lossless reciprocal MiLAC architectures in multi-user networks," *IEEE Wireless Commun. Lett.*, vol. 15, pp. 2609–2613, 2026.
- [4] Z. Wu, M. Nerini, and B. Clerckx, "Microwave linear analog computer (MiLAC)-aided multiuser MISO: Fundamental limits and beamforming design," *arXiv preprint arXiv:2601.10060*, 2026.
- [5] X. Zhou, T. Fang, Y. Mao, and B. Clerckx, "Two-layer microwave linear analog computer (MiLAC)-aided multi-user MISO networks," *arXiv preprint arXiv:2604.24303*, 2026.
- [6] Y. Zhang, P. Zheng, and T. Y. Al-Naffouri, "Quantization-aware EE optimization and SE-EE tradeoff for milac-aided MU-MISO beamforming," *arXiv preprint arXiv:2604.24538*, 2026.
- [7] Z. Liu, Z. Wu, and B. Clerckx, "Microwave linear analog computer (MiLAC)-aided MIMO radar sensing: Transmit beamforming design and DoA estimation," *arXiv preprint arXiv:2605.21020*, 2026.
- [8] Q. Wu and R. Zhang, "Intelligent reflecting surface enhanced wireless network via joint active and passive beamforming," *IEEE Trans. Wireless Commun.*, vol. 18, no. 11, pp. 5394–5409, 2019.
- [9] Q. Wu, S. Zhang, B. Zheng, C. You, and R. Zhang, "Intelligent reflecting surface-aided wireless communications: A tutorial," *IEEE Trans. Commun.*, vol. 69, no. 5, pp. 3313–3351, 2021.
- [10] X. Mu, Y. Liu, L. Guo, J. Lin, and R. Schober, "Simultaneously transmitting and reflecting (STAR) RIS aided wireless communications," *IEEE Trans. Wireless Commun.*, vol. 21, no. 5, pp. 3083–3098, 2022.
- [11] S. Shen, B. Clerckx, and R. Murch, "Modeling and architecture design of reconfigurable intelligent surfaces using scattering parameter network analysis," *IEEE Trans. Wireless Commun.*, vol. 21, no. 2, pp. 1229–1243, 2022.
- [12] H. Li and B. Clerckx, "Non-reciprocal beyond diagonal RIS: Multipoint network models and performance benefits in full-duplex systems," *IEEE Trans. Commun.*, vol. 73, no. 11, pp. 12 221–12 234, 2025.
- [13] D. M. Pozar, *Microwave engineering*. John Wiley & Sons, 2011.
- [14] M. Nerini, S. Shen, and B. Clerckx, "Closed-form global optimization of beyond diagonal reconfigurable intelligent surfaces," *IEEE Trans. Wireless Commun.*, vol. 23, no. 2, pp. 1037–1051, 2024.